Abstract

This paper presents an overview of the steady and harmonic adjoint methods for turbomachinery design using the 'discrete' approach in which the discretized nonlinear Euler/Navier-Stokes equations are linearized and the resulting matrix is then transposed. Steady adjoint solvers give the linear sensitivity of steady-state functionals such as mass flow and average exit flow angle to arbitrary changes in the geometry of the blades and this linear sensitivity information can then be used as part of a nonlinear optimization procedure. The harmonic adjoint method is based on a single frequency of unsteadiness and allows one to determine the generalized force acting on the blades due to arbitrary incoming time-periodic gusts. When the forcing is due to the wakes of the upstream blades the adjoint approach can be used to tailor the shape of the incoming wakes to greatly reduce the level of forced vibration they induce. The presented suite of test-cases includes the Inlet Guide Vane and the rotor of a High Pressure Turbine.

Adjoint Calculation of Sensitivities of Turbomachinery Objective Functions

M.Sergio Campobasso, * Mihai C. Duta, † Michael B. Giles ‡

Oxford University Computing Laboratory

Oxford, UK

May 19, 2003

*Research Officer, OUCL, Parks Road, OX1 3QD Oxford, UK

†Research Officer, OUCL, Parks Road, OX1 3QD Oxford, UK

‡Professor of Computational Fluid Dynamics, OUCL, Parks Road, OX1 3QD Oxford, UK

1 Introduction

Modern turbomachinery has to meet exacting standards of efficiency resulting in low weight and highly loaded engine components. For this reason, the numerical methods for design optimization of fans, compressors and turbines are becoming increasingly popular in the turbomachinery industry. Multidisciplinary design systems allow the designer to modify blade and end-wall geometries in order to optimize the steady aerodynamic performance [1] fulfilling appropriate mechanical constraints. A typical example is the minimum cross section of the blade, which cannot be reduced below a minimum threshold to prevent the steady working stress from exceeding the material strength. However, even if the redesigned blade fulfills the steady stress requirements, it may still be subject to critical unsteady stresses due to the blade *forced response* [2]. This aeroelastic phenomenon is caused by the relative motion of adjacent frames of reference, which transforms steady circumferential variations of the flow field in one frame into periodic time-varying forces acting on the blades in the other. The resulting forced vibration may lead to High Cycle Fatigue, which may shorten the life of the blades below the target life of the engine. This and similar other issues motivate the growing interest of the turbomachinery community in the *unsteady design* methods. By this expression, one means designing components which can better withstand unsteady aeroelastic loads, such as those due to forced response.

Several functionals can be envisaged for the optimization of the steady design. One obvious choice would be the stage efficiency, which in turn depends on the exit loss. However, the secondary kinetic energy [1] is often preferred, being less affected than the loss by possible inaccuracies associated with the turbulence mod-

els. Other objective functions include the mass flow and the radial distribution of the exit-plane whirl angle. The formulation of the unsteady design problem is less trivial. Over the past two decades, a number of methods have emerged to carry out the analysis of turbomachinery aeroelasticity, varying from uncoupled linearized potential flow solvers [3, 4] to fully-coupled nonlinear three-dimensional unsteady viscous methods [5].Within this range, the uncoupled linear harmonic Euler and Navier-Stokes (NS) methods have proved to be a successful compromise between accuracy and cost [6, 7, 8, 9]. This approach views the aerodynamic unsteadiness as a small perturbation of the space-periodic mean steady flow. Hence the unsteady flow field can be linearized about it and due to linearity can be decomposed into a sum of harmonic terms, each of which can be computed independently. The cyclic periodicity of both the steady and unsteady flow leads to a great reduction of computational costs, since the analysis can focus on one blade passage rather than the whole blade-row making use of suitable periodic boundary conditions [9]. In the linear analysis of blade forced response the harmonic component under investigation is that whose frequency is closest to the mechanical frequency of a particular structural mode (near-resonance conditions) and the output of interest is the *worksum* functional [2]. In the context of Lagrangian mechanics, the worksum corresponds to the generalized force acting on the blades for a particular structural mode of vibration due to the linear flow unsteadiness and is therefore the obvious choice for the objective function to be minimized in the unsteady design problem. When the forced response is caused by the wakes shed by an upstream blade-row, the design space is that associated with the shape of the incoming wakes and each wake corresponds to a particular design of the

upstream blades.

The nonlinear gradient-based optimization of the steady design requires the sensitivities of the objective function to a set of m design variables at each step of the optimization. One way of accomplishing this, is to calculate m nonlinear flow fields associated with m perturbed geometries and determine the gradient of the functional by finite-differencing. Conversely the use of adjoint equations [10] allows one to determine all m components of the gradient with a single adjoint computation, at a cost comparable with that of a single solution of the nonlinear flow equations. In the forced response problem, one may want to tailor the shape of the incoming wakes to minimize the forced response of the downstream blades. In the context of the linear unsteady analysis, this would require the solution of the linearized equations for each wake considered. On the other hand, the use of the harmonic adjoint equations [2, 11] provides the generalized force on the blade due to an arbitrary wake with a single harmonic adjoint calculation at a cost comparable with that of the solution of the linear harmonic equations. Thus the computationally most demanding phase of the optimization process requires only two CFD calculations, which are the solution of the mean steady flow field and that of the harmonic adjoint equations. Florea and Hall [12] applied the adjoint method to compute the sensitivity of blade loads to an incoming gust. Two-dimensional inviscid unsteady flow applications were considered and the approach was successively used for three-dimensional inviscid flows [13] and two-dimensional viscous problems [14]. In this paper the extension of the adjoint technique to three-dimensional steady and unsteady viscous flows will be presented.

The adjoint technique for optimal aeronautical design has been pioneered by

Jameson for the potential flow, Euler and NS equations [15, 16, 17]. A number of other research groups have also developed adjoint CFD codes [18, 19, 20] using the same 'continuous' approach in which the first step is to linearize the original partial differential equations. Then the adjoint equations and appropriate boundary conditions are formulated and finally discretized. The alternative 'discrete' approach, which we use, takes a discretization of the NS equations, linearizes the discrete equations and then uses the transpose of the linear operator to form the adjoint problem. This approach has been developed by Elliott and Peraire [21, 22], Anderson and Bonhaus [23], Nielsen and Anderson [24], Mohammadi and Pironneau [25] and Kim *et al.* [26] for external aerodynamic applications. One of the advantages of the discrete approach is that the linear code can be validated by direct comparison with the nonlinear code. Similarly, since the adjoint code is obtained by transposing the linear operator, it must produce exactly the same output both at the routine level and for the objective function. These features enable one to validate the adjoint against the linear code. Furthermore both the linearization of the nonlinear discrete equations and the implementation of the adjoint code can be performed by automatic differentiation software, greatly reducing the development effort. A more detailed comparison between the continuous and the discrete adjoint approach can be found in [27].

The HYDRA suite of 3D Euler/NS codes includes nonlinear, linear and adjoint solvers for external and internal flows. These codes approximate the flow equations on unstructured hybrid grids with an edge-based discretization and they make use of MPI-based distributed parallel computing. The main objectives of this paper are to *a*) summarize the implementation of the discrete adjoint method

in the HYDRA framework and *b*) demonstrate the effectiveness of the adjoint approach for obtaining the linear sensitivities of steady and unsteady functionals at a greatly reduced computational cost when dealing with high-dimensional design spaces. Presented results include the application of the adjoint method to a suite of realistic turbomachinery test cases.

2 Adjoint approach

We start by considering the discrete nonlinear steady Euler equations with a weak imposition of boundary conditions on solid walls enforced specifying zero mass flux through the faces on the surface. As discussed in the next section, the inflow, outflow and periodic boundary conditions are also treated specifying appropriate fluxes and therefore the discrete system of equations which is solved has the form:

$$\mathbf{R}(\mathbf{U}(\mathbf{z}), \mathbf{X}(\mathbf{z})) = 0\,. \tag{1}$$

Here the vector $\mathbf{R}$ represents the discrete flux residuals, $\mathbf{U}$ is the vector of primitive flow variables, $\mathbf{X}$ is the vector of nodal coordinates and $\mathbf{z}$ is a set of m design variables which controls the geometry of the blade. Note that both $\mathbf{U}$ and $\mathbf{X}$ depend on $\mathbf{z}$, because the computational mesh deforms conforming to the current geometry of the blade being designed. The nodal displacements are determined using the *spring analogy* [2], namely modeling the grid edges as springs with spring constants inversely proportional to their length, enforcing suitable perturbations at the nodes on the blade surface.

Linearizing equations (1) with respect to the perturbation of each design vari-

able z_i yields

$$L\hat{\mathbf{u}}_i = \mathbf{f}_i \ , \quad i = 1, \ldots, m \ ,$$

where

$$L \equiv \frac{\partial \mathbf{R}}{\partial \mathbf{U}}, \quad \hat{\mathbf{u}}_i \equiv \frac{d\mathbf{U}}{dz_i}, \quad \mathbf{f}_i \equiv -\frac{\partial \mathbf{R}}{\partial z_i} \ .$$

The corresponding m perturbations of a nonlinear functional $J(\mathbf{U}(\mathbf{z}), \mathbf{z})$ are:

$$\widetilde{J}_i \equiv \frac{dJ}{dz_i} = \mathbf{g}^T \hat{\mathbf{u}}_i + \frac{\partial J}{\partial z_i} \ , \quad i = 1, \ldots, m \ , \tag{2}$$

where

$$\mathbf{g}^T \equiv \frac{\partial J}{\partial \mathbf{U}} \ .$$

Using the adjoint approach, the m sensitivities can be obtained by evaluating

$$\widetilde{J}_i = \mathbf{v}^T \mathbf{f}_i + \frac{\partial J}{\partial z_i} \ , \quad i = 1, \ldots, m \ , \tag{3}$$

where the adjoint solution $\mathbf{v}$ satisfies the equation

$$L^T \mathbf{v} = \mathbf{g} \ .$$

The equivalence of this formulation comes from the following identity:

$$\mathbf{g}^T \hat{\mathbf{u}}_i = \mathbf{g}^T L^{-1} \, \mathbf{f}_i = \left((L^T)^{-1} \mathbf{g} \right)^T \mathbf{f}_i = \mathbf{v}^T \mathbf{f}_i \ .$$

Each design variables gives rise to a different vector $\mathbf{f_i}$, whereas if there is only one functional J, there is only one vector $\mathbf{g}$. Thus the adjoint approach requires just one adjoint calculation to obtain the sensitivity of one objective function to any number of design variables. On the other hand, the linear approach would require m solutions of the linearized flow equations to obtain the m flow fields $\hat{\mathbf{u}}_i$. (Note that the vectors $\mathbf{f_i}$ and $\mathbf{g}$ are determined in a computationally cheap preprocessing step).

In the forced response problem, the linear harmonic equations are complex and the linearized functional $\widetilde{J}_i$ corresponds to the worksum integral w_i, which represents the generalized force acting on the blade for a particular structural mode [2]. Denoting by ^{H} the Hermitian conjugate operator, one has:

$$\widetilde{J}_i = \mathbf{v}^H \mathbf{f}_i = w_i \ . \tag{4}$$

The vector $\mathbf{f_i}$ depends only on the incoming gust and hence the blade forced response can be computed for any source of aerodynamic unsteadiness, once the solution $\mathbf{v}$ of the harmonic adjoint equations has been determined. In this case, the grid does not deform and consequently the term $\frac{\partial J}{\partial z_i}$ appearing in equations (2) and (3) is identically zero and so does not appear in equation (4).

Finally note that the elements of the vector $\mathbf{g}$ are non-zero only at nodes where the objective function is defined, at the nodes on the outlet plane if the functional is the exit mass flow and at the nodes on the blade surface if the functional is the worksum integral. The analysis of the nonlinear, linear and adjoint equations is carried out in greater detail in the three following sections.

3 Nonlinear flow analysis

The discrete nonlinear analysis of the time-averaged flow field is applied to a single turbomachinery blade-row in the relative frame of reference. The flow can be modeled by either the Euler or the Reynolds–averaged NS equations coupled with the Spalart–Almaras turbulence model. Due to the rotational speed, source terms associated with the centrifugal and Coriolis forces appear in the momentum equations. Denoting by $\overline{\mathbf{U}}$ and $\overline{\mathbf{X}}$ the unperturbed flow field and nodal coordinates

respectively, these terms can all be formally included in the equation

$$\mathbf{R}(\overline{\mathbf{U}}, \overline{\mathbf{X}}) = 0\,. \tag{5}$$

Because the governing equations are approximated on an unstructured grid using an edge-based algorithm [28, 29], the residual vector $\mathbf{R}$ is a sum of contributions from all of the edges of the grid, with each edge contributing only to the residuals corresponding to the two nodes at either end. The nonlinear system (5) has size $(N_{eqs} \times N)$, where N is the number of grid nodes, $N_{eqs} = 5$ for the inviscid flow model and $N_{eqs} = 6$ for turbulent flows. The 6^{th} component in the latter case is the turbulence variable, determined with the Spalart-Almaras turbulence model.

The boundary conditions to which the system (5) is subject can be of three types: inflow/outflow, periodic and inviscid/viscous wall. The inflow and outflow boundaries are handled through fluxes which incorporate prescribed flow information and thus they become part of the residual vector $\mathbf{R}$. At matching pairs of periodic nodes the periodicity condition for linear cascades is enforced setting the flow state on the upper boundary equal to that on its lower counterpart. In the case of annular domains because of the use of Cartesian coordinates, the velocity vectors on the upper boundary are obtained by rotating those on the lower one. Combining flux residuals at the two periodic nodes in a suitable manner to maintain periodicity, this boundary condition can also be included in the definition of the flux residual vector $\mathbf{R}$. A no-slip boundary condition is applied to viscous walls discarding the momentum residuals and replacing these equations by the specification of zero velocity at the boundary nodes. The computation of the flux residuals at nodes on inviscid walls is based on zero mass flux through the boundary faces, but in addition flow tangency is enforced by setting the normal component of the

surface velocity to zero and disregarding the normal component of the momentum residuals. Applying these *strong wall boundary conditions* [27] to the system (5) yields:

$$(I-B)\ \mathbf{R}(\overline{\mathbf{U}}) \;=\; 0 \tag{6}$$

$$B\ \overline{\mathbf{U}} \;=\; 0 \tag{7}$$

where B is the projector which extracts the normal momentum/velocity components at the nodes on inviscid wall boundaries and the whole momentum/velocity at the nodes on viscous walls. The square matrix associated with the linear operator B has size $((N \times N_{eqs}) \times (N \times N_{eqs}))$ and is block-diagonal with each block of size $(N_{eqs} \times N_{eqs})$. The matrix B has only n_w nonzero blocks, n_w being the overall number of nodes on wall boundaries. Denoting by $\mathbf{n}_w$ the wall normal and by (n_x, n_y, n_z) its components, the generic form of the diagonal block in the inviscid and viscous case is

$$\begin{bmatrix} 0 & 0 & 0 & 0 & 0 \\ 0 & n_x^2 & n_x n_y & n_x n_z & 0 \\ 0 & n_y n_x & n_y^2 & n_y n_z & 0 \\ 0 & n_z n_x & n_z n_y & n_z^2 & 0 \\ 0 & 0 & 0 & 0 & 0 \end{bmatrix} \qquad \text{and} \qquad \begin{bmatrix} 0 & 0 & 0 & 0 & 0 \\ 0 & 1 & 0 & 0 & 0 \\ 0 & 0 & 1 & 0 & 0 \\ 0 & 0 & 0 & 1 & 0 \\ 0 & 0 & 0 & 0 & 0 \end{bmatrix} \tag{8}$$

respectively.

The discrete equations (6) and (7) are solved using Runge-Kutta time-marching accelerated by Jacobi preconditioning and multigrid. Further details on the implementation of the nonlinear solver can be found in references [28, 2].

4 Linear flow analysis

Both the variations of the steady flow due to geometric perturbations and the flow unsteadiness due to incoming gusts are treated as small linear perturbations. In the steady case, one deliberately uses small perturbations to obtain an accurate estimate of the gradient. Assuming that the flow unsteadiness can also be treated as a small perturbation of the mean steady flow field, one can carry out a linear analysis of the perturbed flow field in both the steady and unsteady case. Note that forced response is not a fundamentally linear phenomenon, because it is always characterized by a finite level of unsteadiness and it is not clear *a priori* that linear perturbation methods should give accurate predictions. However a series of studies based on the comparison of nonlinear and linear results [6, 30, 31, 32] as well as linear results and experimental data [33] point to the suitability of the linear approach for turbomachinery forced response.

In the steady design problem, the perturbation of a single design variable z induces a flow perturbation $\hat{\mathbf{u}} \equiv d\mathbf{U}/dz$ and the perturbed flow field $\mathbf{U}$ can be written as

$$\mathbf{U} = \overline{\mathbf{U}} + \hat{\mathbf{u}}, \qquad ||\hat{\mathbf{u}}|| \ll ||\overline{\mathbf{U}}||$$

In the forced response problem, the time-periodicity of the unsteadiness implies that the linear time-dependent component of the flow can be written as a sum of harmonics, each of which can be analyzed independently due to linearity. Considering just the fundamental harmonic of frequency ω, the unsteady flow field $\mathbf{U}(\mathbf{t})$ can be written as the sum of the mean steady nonlinear flow field $\overline{\mathbf{U}}$ and the real part of the small harmonic perturbation of known frequency ω and unknown

complex amplitude $\hat{\mathbf{u}}$:

$$\mathbf{U}(t) = \overline{\mathbf{U}} + \mathcal{R}\{\exp(\mathrm{i}\omega t)\ \hat{\mathbf{u}}\}. \tag{9}$$

The complex vector $\hat{\mathbf{u}}$ represents the amplitude and phase of the unsteady flow.

The governing equations for the flow perturbation $\hat{\mathbf{u}}$ are formally identical in the steady and unsteady case, since the linearization of both the discrete steady equations (6) and (7) and their unsteady counterpart [9] leads to the linear system:

$$(I-B)\left[(i\omega + L)\hat{\mathbf{u}} - \mathbf{f}\right] = 0 \tag{10}$$

$$B\ \hat{\mathbf{u}} = \hat{\mathbf{u}}_{wall}\ . \tag{11}$$

in which the linear operator $L \equiv \frac{\partial \mathbf{R}}{\partial \mathbf{U}}$ gives the sensitivity of the discrete nonlinear residual $\mathbf{R}$ to the flow perturbation $\hat{\mathbf{u}}$. The perturbation $\hat{\mathbf{u}}_{wall}$ of the wall velocity is zero for viscous walls and its general form in the case of stationary and moving inviscid walls is derived in reference [2].

In the steady problem, the frequency ω is zero and the system of equations (10) and (11) is defined in the real domain. The source term $\mathbf{f} \equiv -\partial\mathbf{R}/\partial z$ provides the sensitivity of the residual vector $\mathbf{R}$ to the grid perturbation and is non-zero throughout the computational domain. An accurate estimate of $\mathbf{f}$ is obtained using the complex variable method described in [27]. In order to ensure the full consistence of the steady functionals (which depend on the solution of the nonlinear flow equations) with their linear sensitivities (which additionally depend on the solution of the linearized flow equations), a completely reflective treatment of the far-field boundaries is adopted: the inflow and outflow boundary conditions are obtained by linearizing their nonlinear counterparts, that is setting to zero the appropriate linearized far-field information. For example, the linearized total

pressure, total temperature and flow angle perturbations are set to zero at a subsonic inflow boundary. The linear periodic boundary condition is the same as for the nonlinear equations.

In the forced response case, the system of linear harmonic equations (10) and (11) defining the unsteady flow perturbation is complex and can be viewed as the frequency domain counterpart of the nonlinear unsteady equations. When the incoming gust is the wake shed by the upstream blade-row, the source term $\mathbf{f}$ is non-zero only at the inflow boundary and it depends on the radial distribution of the complex coefficients of the first harmonic of the wake. To leading order, the amplitude of these coefficients depends on the circumferential width of the wake, while their phase provides the circumferential postion. The far-field boundaries are treated with a linearized free-stream boundary condition enforced by setting to zero the flow perturbation $\hat{\mathbf{u}}$ and its implementation is based on nonreflecting boundary conditions to minimize spurious reflections [34]. The periodic boundary conditions for the complex flow field $\hat{\mathbf{u}}$ are a generalization of their steady counterpart, obtained introducing the inter-blade phase angle φ ($IBPA$). This is a complex phase shift $\exp(\mathrm{i}\varphi)$ between the flow field at the lower and upper periodic boundaries. In the forced response problem, it arises when the wakes and blades have different pitches and therefore there is a difference in the times at which neighbouring wakes strike neighbouring blades.

The linear equations are solved with the same pseudo time-marching approach adopted for the solution of the nonlinear steady equations, that is by introducing and discretizing a fictitious time-derivative $d\hat{\mathbf{u}}/d\tau$ in the system of equations (10) and (11) and time-marching the solution of the preconditioned system until a

'steady state' is achieved. Viewing the linearized flow equations as the linear system $A\mathbf{x} = \mathbf{b}$, this procedure can be regarded as the preconditioned fixed-point iteration

$$\mathbf{x}_{n+1} = (I - M^{-1}A)\mathbf{x}_n + M^{-1}\mathbf{b} \,, \tag{12}$$

in which M^{-1} is a preconditioning matrix resulting from the Runge-Kutta time-marching algorithm, the Jacobi preconditioner and one multigrid cycle. The iterative equation (12) converges if all the eigenvalues of $M^{-1}A$ lie in the unit disc centred at $(1, 0)$ in the complex plane and this condition is fulfilled for most aeroelastic problems of practical interest. However in some cases the nonlinear base flow used for the linearization is characterized by small-amplitude limit cycles related to some physical phenomenon such as small separation bubbles or vortex shedding. These flow instabilities result in a usually small number of complex conjugate pairs of outliers of the preconditioned linear operator, that prevent the standard iteration (12) from converging. In such cases convergence can be retrieved only by solving the linear equations with algorithms which are guaranteed to work even in the presence of outliers. The *Generalized Minimum Residuals* (GMRES) algorithm [35] and the *Recursive Projection Method* [36] belong to this category and a detailed description of their use in the linear code is provided in references [9, 37].

5 Adjoint Flow Analysis

The steady and harmonic adjoint equations are formally identical as they are both obtained by transposing the linearized flow equations. The only practical difference is that the steady adjoint problem is defined in the real domain with zero frequency

and IBPA, while the harmonic adjoint system is defined in the complex domain with a nonzero frequency ω and IBPA φ. In the following analysis we use the Hermitian operator ^{H} for both problems, with the implicit assumption that this reduces to the transpose operator ^{T} for the steady equations.

In order to determine the adjoint flow equations we start by adding equations (10) and (11). This yields:

$$\left[(I-B)(i\omega+L)+B\right]\ \hat{\mathbf{u}} = (I-B)\,\mathbf{f} + \hat{\mathbf{u}}_{\mathbf{wall}}\,. \tag{13}$$

The appropriate adjoint equation is then found by taking the Hermitian conjugate of the linear operator and since the boundary operator B is symmetric this yields:

$$\Big((i\omega+L)^H(I-B)+B\Big)\,\mathbf{v} = \mathbf{g}\,. \tag{14}$$

At this point it is convenient to decompose both $\mathbf{v}$ and $\mathbf{g}$ into orthogonal components as

$$\mathbf{v} = (I-B)\mathbf{v} + B\mathbf{v} \quad = \mathbf{v}_{||} + \mathbf{v}_{\perp}\,,$$

$$\mathbf{g} = (I-B)\mathbf{g} + B\mathbf{g} \quad = \mathbf{g}_{||} + \mathbf{g}_{\perp}\,.$$

Pre-multiplying equation (14) by $(I-B)$ and noting that B is idempotent (i.e. $B^2=B$) shows that $\mathbf{v}_{||}$ satisfies the system

$$(I-B)(i\omega+L)^H\mathbf{v}_{||} \quad = \mathbf{g}_{||}\,, \tag{15}$$

$$B\,\mathbf{v}_{||} \quad = 0\,. \tag{16}$$

These are the equations which are solved iteratively by the adjoint code. Once $\mathbf{v}_{||}$ has been computed, $\mathbf{v}_{\perp}$ is calculated in a post-processing step using an equation obtained by pre-multiplying equation (14) by B:

$$\mathbf{v}_{\perp} = \mathbf{g}_{\perp} - B(i\omega+L)^H\mathbf{v}_{||}\,. \tag{17}$$

In the steady problem, the linearized functional is given by

$$\widetilde{J} = \mathbf{v}^T \left((I - B)\mathbf{f} + \hat{\mathbf{u}}_{wall} \right) + \frac{\partial J}{\partial z} = \mathbf{v}_{\parallel}^T \mathbf{f} + \mathbf{v}_{\perp}^T \hat{\mathbf{u}}_{wall} + \frac{\partial J}{\partial z} \, .$$

This shows that $\mathbf{v}_{\perp}$ gives the sensitivity of the functional to the linearized wall velocity $\hat{\mathbf{u}}_{wall}$. Note that $\mathbf{v}_{\perp}$ does *not* correspond to the normal momentum component of the analytic adjoint solution at the boundary. In the forced response problem, the worksum functional is

$$\widetilde{J} \equiv w = \mathbf{v}^{\mathbf{H}} \mathbf{f} = \mathbf{v}_{\parallel}^{\mathbf{H}} \mathbf{f} \, ,$$

since there is no grid perturbation and the linearized wall velocity $\hat{\mathbf{u}}_{wall}$ is zero in both the inviscid and viscous case [2].

It is not obvious how best to solve the adjoint equations. Using the same iterative method as for the nonlinear and linear equations (except with the transpose of the Jacobi preconditioning matrix) was found to work well for inviscid flows, but there were significant stability problems with viscous flows. To overcome these, Giles analyzed the iterative evolution of the output functional, finding that the adjoint code can be designed to give exactly the same iterative history as the linear code in terms of the output functional. This is achieved by properly constructing an adjoint version of the usual Runge-Kutta algorithm and using adjoint restriction and prolongation operators for the multigrid [38]. In this way, the stability and the iterative convergence rate of the adjoint code are identical to those of the linear code, because this procedure makes the preconditioned adjoint operator the exact transpose of the preconditioned linear operator and consequently they have the same eigenvalues. The convergence rate of the linear code is in turn equal to the asymptotic convergence rate of the nonlinear code for $IBPA = 0$

and $\omega \to 0$. The same GMRES solver implemented in the linear code has also been used for solving the adjoint equations (15) and (16) in the presence of small-amplitude limit cycles in the underlying base flow solution, to avoid the numerical instabilities which would otherwise affect the standard fixed-point iteration.

The linearization of the nonlinear code and the implementation of the adjoint code of the HYDRA suite have been carried out manually. This requires a bigger development effort than using automatic differentiation tools [39], but it allows one to minimize the CPU time per multigrid iteration. The CPU cost per iteration for the steady adjoint code is only 10-20% greater than for the nonlinear code. The memory requirements are 20-30% greater than for the nonlinear code, depending on the grid that is used. More details on the optimization of the adjoint implementation are provided in reference [27].

6 Validation

Using the discrete adjoint method, each routine of the adjoint code is the exact transpose of its counterpart in the linear code [40, 27]. Therefore the validation of the adjoint code has been performed at two levels. At the lower level, it has been checked that each adjoint subroutine provides the same output as its linear counterpart. At the higher level, it has been checked that the adjoint and linear codes produce the same value for both the steady and unsteady functionals to machine accuracy at each step of the iterative process. This exact equivalence is one advantage of the fully discrete on the continuous adjoint approach.

The linear code itself has also been checked at a subroutine level by comparison

with the corresponding subroutines in the nonlinear code [40, 27]. In addition it has been validated using a range of test cases, starting with simple model problems such as the inviscid flow over 2D flat plate cascades for which a semi-analytic solution is available [41]. Figure 1 shows the real and imaginary part of the pressure difference across the unstaggered flat plates of a linear cascade due to incoming wakes with $IBPA = -400^0$. Validation of the viscous capabilities is based on benchmark experimental test cases, such as the 2D turbine section of the 11th Standard Configuration, which is the mid-span blade-to-blade section of an annular turbine cascade. Experimental measurements and various computed results of the steady and unsteady flow field due to blade-plunging with prescribed $IBPA$ are provided in reference [42]. The nonlinear mean flow field and the linear flow perturbation have been computed with the nonlinear and linear harmonic HYDRA solvers respectively. All computed results presented in this paper have been obtained using a mesh with 17745 nodes and figure 2 shows a coarser grid with 7869 nodes. Figure 3 provides measured and computed profiles of isentropic Mach number on the blade surface for a transonic working point with exit Mach number of 0.96. The high pressure patch at about 20 % chord and the rapid pressure rise at about 80 % chord on the suction surface (figure 3) are due to a separation bubble and an impinging shock respectively. This is clearly visible in the Mach number contours of figure 4, which also show how both the blade boundary layers and wakes thicken after passing through the shock. The measured and computed amplitude of the linear pressure coefficient for $IBPA = 180^0$ are compared in figure 5-a, while measured and computed values of its phase are shown in figures 5-b. The overall agreement between measured and computed results is

fairly good and the computed results are in a very good agreement with those in the literature [42, 33].

7 Results

In practice, it is often required to monitor both the steady and the unsteady performance. For example, the forced response of a blade-row subject to the constraint of constant circumferential lift can be minimized using steady and harmonic adjoint equations to determine the sensitivities of forced response and lift to variations of the blade geometry [12]. In the context of gradient-based optimization, at least two strategies can be devised to cope with multiple steady and/or unsteady functionals. One approach is to consider a single cost function which is a weighted sum of all functionals. This strategy is often adopted when the design and off-design performance have to be optimized simultaneously [43]. Then numerical unconstrained optimization methods can be used [44]. The alternative approach is to consider a constrained optimization problem in which one functional (steady or unsteady) is treated as objective function and the remaining ones are viewed as constraints. Then constrained optimization techniques such as reduced-gradient-type or projected Lagrangian methods [44] can be applied. Using either approach, one has to determine the sensitivities of each functional at each step of the optimization and this can be accomplished by solving a set of adjoint equations for each functional. The following subsections provide some applications of the adjoint method for determining the sensitivities of steady and unsteady objective functions of turbomachinery interest.

7.1 Two-dimensional turbine section

The first problem consists in determining the sensitivities of two steady functionals to variations of the stagger angle $\Delta\gamma$ of the turbine blades of the 11th standard configuration. The selected objective functions are the mass flow $\dot{m}$ and the quadratic deviation $\Gamma = (\beta - \beta_T)^2$ of the pitchwise averaged exit flow angle β from a target value β_T. The reference flow field associated with the unperturbed geometry is the transonic flow regime discussed in the previous section. Figure 6-a shows the mass flow computed by the nonlinear solver for perturbed geometries obtained letting $\Delta\gamma$ vary between -6^0 and 7.5^0. Note that each circle corresponds to a different nonlinear calculation and positive increments $\Delta\gamma$ lead to higher angles between the blade chord and the axial direction. The nonlinear and the adjoint sensitivities of $\dot{m}$ are compared in figure 6-b. The nonlinear derivative is computed with centred finite-differences on intervals of 1^o and each cross of the curve giving the linear sensitivity corresponds to a particular adjoint calculation based on the nonlinear flow field of the corresponding perturbed geometry. The agreement between the two results is fairly good since the relative difference is about 1% for $\Delta\gamma < -3^0$ and about 2% for $\Delta\gamma \geq -3^0$. The reason why the agreement worsens as $\Delta\gamma$ increases is the growing nonlinearity associated with the separation bubble on the suction side. Increasing the stagger angle results in a higher flow incidence, which in turn widens the separation bubble due to the increased aerodynamic loading. The quadratic deviation Γ of the exit angle computed by the nonlinear code for $\beta_t = 58.6^o$ is plotted versus $\Delta\gamma$ in figure 7-a. The nonlinear and adjoint sensitivities are again in good agreement, as shown in figure 7-b. Though not clearly visible in the plot, a closer inspection of these results shows that the

maximum relative difference between the nonlinear and the adjoint sensitivity is about 3%. The linear sensitivity obtained using the linearized solver is identical to that determined by the adjoint code and therefore has not been reported.

7.2 Turbine Inlet Guide Vane

The second test-case is the Inlet Guide Vane (IGV) of a high-pressure turbine, whose geometry and surface mesh are shown in figure 8. These vanes have a low aspect-ratio and the two end-wall boundary layers meet on the suction side under the sweeping effect of the two passage vortices resulting in a wide region of low total pressure in the centre of the passage. This is clearly visible in the non-dimensional total pressure contours at the outlet plane shown in figure 9. The gas stream becomes sonic in the passage and the pitchwise averaged exit Mach number at blade mid-height is 0.76. The adjoint code has been used to determine the sensitivities of the outlet mass flow to the rotation of 5 blade airfoils around their Trailing Edge (TE), that is to variations of their stagger angle. The blade geometry resulting from the perturbation of the mid-height airfoil is shown in figure 10, whereas figure 11 compares the nonlinear and the adjoint estimates of the 5 mass flow sensitivities. The nonlinear derivatives have been computed with forward finite-differences, using the mass flow determined by 5 nonlinear calculations of the perturbed flow field. The overall agreement of the two estimates is again fairly good, since the relative difference between the nonlinear and linear sensitivities due to the perturbation of the mid-height airfoil is about 3% and becomes slightly higher moving towards the end-walls, due to the nonlinearity of the secondary flows. The linear sensitivities are equal to the adjoint estimates within machine

accuracy and therefore are not reported. We emphasize that a single adjoint calculation is required to determine the 5 linear sensitivities, whereas 5 nonlinear or linear calculations are needed with the finite-difference approach.

7.3 Unsteady design: turbine rotor

The harmonic adjoint method allows one to determine the sensitivity of forced response to the shape of an arbitrary incoming wake, which can be represented by its radial profiles of thickness and circumferential position. Considering only circumferential displacements relative to a reference wake, however, may simplify the redesign of the upstream blade-row. In fact, the new upstream blade may be obtained by re-stacking the given blade-to-blade airfoils according to the displacements of the wake which minimizes forced response, provided that such displacements are sufficiently small. If not, the wake shed by the redesigned blade has to recomputed by means of a nonlinear steady calculation and the search process has to be iterated. The example considered consists of a high pressure turbine rotor whose blades undergo forced response vibrations due to the wakes shed by the upstream stator. This test-case was previously analyzed by Vahdati *et al.* [6], who found a good agreement in the forced response predicted by linear uncoupled and nonlinear coupled methods. Figure 12 shows the blade geometry and surface mesh, whereas figure 13 provides the Mach contours in the mid-height section for the chosen steady working conditions. The wakes which have been analyzed are those obtained by keeping circumferentially fixed the wake close to the hub, shifting the wake close to the tip by a phase shift ξ and linearly interpolating the circumferential position of the wakes in between. This corresponds to a linear

re-stacking of the upstream blades achieved by leaning them in the circumferential direction. The reference wake was extracted by the nonlinear steady flow field of the upstream stator. The adjoint analysis has been used to determine the worksum values corresponding to this set of wakes and identify a minimum response. Figure 14 shows the magnitude of the worksum corresponding to the first torsional mode versus the phase shift ξ and it indicates that the force acting on the blades decreases as $|\xi|$ increases within the range being considered. The physical interpretation of this result is that the maximum structural response occurs when the blades are hit by the wakes at the same time at all radii ($\xi = 0$), whereas the forced response can be reduced by shifting the times at which the wakes hit the blades at different circumferential positions (increasing $|\xi|$).

The results for the full range of phase shifts were obtained from a single harmonic adjoint calculation. Using the standard linear harmonic approach would require a linear calculation for each wake, since each corresponds to a different right-hand-side $\mathbf{f_i}$ for the linear analysis. As a check, linear calculations have been performed for a variety of points and they produced identical values for the worksum output.

8 Conclusions

In this paper the construction of the discrete Euler and NS adjoint equations has been summarized using an algebraic approach and with a strong emphasis on turbomachinery applications. The development of the presented adjoint methods has also involved advances in the methodology for developing and validating fully-

discrete adjoint solvers. This is due to *a*) the exact equivalence of each linear and adjoint routine and *b*) the use of a particular form of Runge-Kutta time-marching scheme for the adjoint equations which gives exact equivalence with the linear code not only in the final results but also during the iterative evolution.

In the framework of gradient-based optimization, the adjoint approach can lead to substantial computational savings when dealing with high-dimensional design spaces. A suite of realistic turbomachinery test-cases has been used to demonstrate the suitability of the adjoint method for obtaining the linear sensitivities of steady and unsteady turbomachinery functionals. The latter is thought to be the first application of the adjoint approach to the linear analysis of three-dimensional viscous blade forced response. The capability of determining the gradient of a scalar objective function depending on many design parameters with a single calculation has a significant potential for application to the design practice in the turbomachinery industry.

Acknowledgements

This research has been supported by the Engineering and Physical Sciences Research Council under grant GR/L95700, and by Rolls-Royce plc (technical monitor: Leigh Lapworth) DERA (technical monitor: John Calvert), and BAESystems plc (technical monitor: David Standingford). We also acknowledge the contributions of P. Moinier, J.-D. Müller, N.A. Pierce, L. Lapworth and M. West to the development of the HYDRA suite of nonlinear, linear and adjoint codes. Prof. Andrea Arnone of the Department of Energy Engineering, University of Florence

(IT), is also kindly acknowledged for providing the grid generation software.

References

[1] Shahpar, S., "A comparative study of optimisation methods for aerodynamic design of turbomachinery blades". ASME Paper 2000-GT-523, May 2000.

[2] Duta, M.C., "The use of the adjoint method for the minimization of forced response," Ph.D. Dissertation, Computing Laboratory, Oxford University, Oxford, UK, March 2002.

[3] Verdon, J.M. and Caspar, J.R., "A linearized unsteady aerodynamic analysis for transonic cascades," *Journal of Fluid Mechanics*, Vol. 149, Dec. 1984, pp. 403–429.

[4] Hall, K.C., "Deforming grid variational principle for unsteady small disturbance flows in cascades," *AIAA Journal*, Vol. 31, No. 5, 1993, pp. 891–900.

[5] Marshall, J.G. and Imregun, M., "A review of aeroelasticity methods with emphasis on turbomachinery applications," *Journal of Fluid and Structures*, Vol. 10, 1996, pp. 237–267.

[6] Vahdati, M., Green, J., Marshall, J.G. and Imregun, M., "Forced response predictions for a HP turbine rotor blade," *Proceedings of the Symposium on Design Principles and Methods for Aircraft Gas Turbine Engines*, NATO Research and Technology Organization, Neuilly-Sur-Seine, France, 1999.

[7] Hoyniak, D. and Clark, W.S., "Aerodynamic damping predictions using a linearized Navier-Stokes analysis", ASME Paper 99-GT-207, June 1999.

[8] Clark, W.S. and Hall, K.C., "A time-linearized Navier-Stokes analysis of stall flutter," *Journal of Turbomachinery*, Vol. 122, No. 3, July 2000, pp. 467– 476.

[9] Campobasso, M.S. and Giles, M.B., "Effect of flow instabilities on the linear analysis of turbomachinery aeroelasticity," *AIAA Journal of Propulsion and Power*, Vol. 19, No. 2, 2003, pp. 250–259.

[10] Giles, M.B., "Aerodynamic design optimization for complex geometries using unstructured grids," *Inverse design and optimisation methods, VKI Lecture Series 1997-05.* von Karman Institute for Fluid Dynamics, Rhode-St-Genese, Belgium, 1997.

[11] Duta, M.C., Giles, M.B. and Campobasso, M.S., "The harmonic adjoint approach to unsteady turbomachinery design," *International Journal for numerical methods in fluids*, Vol. 40, October 2002, pp. 323–332.

[12] Florea, R. and Hall, K.H., "Sensitivity analysis of unsteady inviscid flow through turbomachinery cascades," *AIAA Journal*, Vol. 39, No. 6, 2001, pp. 1047–1056.

[13] Hall, K.C. and Thomas, J.P., "Sensitivity analysis of coupled aerodynamic/structural dynamic behavior of blade rows," *Proceedings of the 7th National Turbine Engine High Cycle Fatigue (HCF) Conference*, Universal Technology Corporation, Dayton, OH, 2002.

[14] Thomas, J.P. and Hall, K.H., "A Discrete Adjoint Approach for Modelling Unsteady Aerodynamic Design Sensitivities," AIAA Paper 2003-0041, January 2003.

[15] Jameson, A., "Aerodynamic design via control theory," *Journal of Scientific Computing*, Vol. 3, 1988, pp. 233–260.

[16] Jameson, A., "Optimum aerodynamic design using control theory," *Computational Fluid Dynamics Review 1995*, Hafez, M. and Oshima, K. editors, John Wiley & Sons, 1995, pp. 495–528.

[17] Jameson, A., "Re-engineering the design process through computation," *Journal of Aircraft*, Vol. 36, No. 1, 1999, pp. 36–50.

[18] Baysal, O. and Eleshaky,E.M., "Aerodynamic design optimization using sensitivity analysis and computational fluid dynamics," *AIAA Journal*, Vol. 30, No. 3, 1992, pp. 718–725.

[19] Dadone, A. and Grossman, B., "Progressive optimization of inverse fluid dynamic design problems," *Computers and Fluids*, Vol. 29, No. 1, 2000, pp. 1–32.

[20] Korivi, V.M., Taylor III, A.C. and Hou, G.W., "Sensitivity analysis, approximate analysis and design optimization for internal and external viscous flows," AIAA Paper 91-3083, September 1991.

[21] Elliott, J. K. and Peraire, J., "Practical three-dimensional aerodynamic design and optimization using unstructured meshes," *AIAA Journal*, Vol. 35, No. 9, 1997, pp. 1479–1485.

[22] Elliott, J.K., "Aerodynamic optimization based on the Euler and Navier–Stokes equations using unstructured grids," Ph.D. Dissertation, Department of Aeronautics and Astronautics, Massachusetts Institute of Technology, Cambridge, USA, May 1999.

[23] Anderson, W. K. and Bonhaus, D. L., "Airfoil design on unstructured grids for turbulent flows," *AIAA Journal*, Vol. 37, No. 2, 1999, pp. 185–191.

[24] Nielsen, E. J. and Anderson, W. K., "Aerodynamic design optimization on unstructured meshes using the Navier–Stokes equations," *AIAA Journal*, Vol. 37, No. 11, 1999, pp. 1411–1419.

[25] Mohammadi, B. and Pironneau, O., "Mesh adaption and automatic differentiation in a CAD-free framework for optimal shape design," *International Journal for Numerical Methods in Fluids*, Vol. 30, No. 2, 1999, pp. 127–136.

[26] Kim, H.J., Sasaki, D., Obayashi, S. and Nakahashi, K., "Aerodynamic optimization of supersonic transport wing using unstructured adjoint methods," *Proceedings of the International Conference of Computational Fluid Dynamics*, Springer Verlag, Berlin, Germany, 2001, pp. 581–588.

[27] Giles, M.B., Duta, M.C., Mueller, J.D. and Pierce, N.A., "Algorithm developments for discrete adjoint methods," *AIAA Journal*, Vol. 41, No. 2, 2003, pp. 198–205.

[28] Moinier, P., "Algorithm developments for an unstructured viscous flow solver," Ph.D. Dissertation, computing Laboratory, Oxford University, Oxford, UK, December 1999.

[29] Moinier, P. Mueller, J.D. and Giles, M.B., "Edge-based multigrid and preconditioning for hybrid grids," *AIAA Journal*, Vol. 40, No. 10, 2002, pp. 1954–1960.

[30] Marshall, J.G. and Giles, M.B., "Some applications of a time-linearised Euler method to flutter and forced response in turbomachinery," *Proceedings*

of the 8th International Symposium on Unsteady Aerodynamics, Aeroacoustics and Aeroelasticity in Turbomachines, Kluwer Academics, Dordrecht, The Netherlands, 1998, pp. 225–240.

[31] Suddhoo, A., Giles, M.B. and Stow, P., "Simulation of inviscid blade row interaction using a linear and nonlinear method," ISABE Paper 91-7049, September 1991.

[32] Manwaring, S.R. and Wisler, D.C., "Unsteady aerodynamics and gust response in compressors and turbines," *Journal of Turbomachinery*, Vol. 115, No. 4, October 1993, pp. 724–740.

[33] Sbardella, L. and Imregun, M., "Linearized unsteady viscous turbomachinery flows using hybrid grids," *Journal of Turbomachinery*, Vol. 123, No. 3, July 2001, pp. 568– 582.

[34] Giles, M.B., "Nonreflecting boundary conditions for Euler equation calculations," *AIAA Journal*, Vol. 28, No. 12, 1990, pp. 2050–2058.

[35] Saad, Y. and Schultz, M.H., "GMRES: a generalized minimal residual algorithm for solving nonsymmetric linear systems," *SIAM Journal on Scientific and Statistical Computing*, Vol. 7, No. 3, 1986, pp. 856–869.

[36] Shroff, G.M. and Keller, H.B., "Stabilization of unstable procedures: the Recursive Projection Method," *Journal of Applied Mathematics*, Vol. 30, No. 4, 1993, pp. 1099-1120.

[37] Campobasso, M.S. and Giles, M.B., "Stabilization of a linearized Navier-Stokes solver for turbomachinery aeroelasticity," *Proceedings of the 2nd In-*

ternational Conference on Computational Fluid Dynamics, Springer Verlag, Berlin, Germany, 2003, pp. 343–348.

[38] M.B. Giles. "On the use of Runge-Kutta time-marching and multigrid for the solution of steady adjoint equations," Technical Report NA00/10, Oxford University Computing Laboratory, UK, June 2000.

[39] Giering, R. and Kaminski, T., "Recipes for adjoint code construction," *ACM Transactions on Mathematical Software*, Vol. 24, No. 4, 1998, pp. 437–474.

[40] Giles, M.B. and Pierce, N.A., "An introduction to the adjoint approach to design," *Flow, Turbulence and Control*, Vol. 65, No. 3/4, 2001, pp. 891–900.

[41] Whitehead, D.S., "Classic two-dimensional methods," *Aeroelasticity in Axial-Flow Turbomachines, AG-298*, Platzer, M. and Carta, F.O. editors, Vol. 1. AGARD, 1987.

[42] Fransson, T.H., Joeker, M., Boelcs, A. and Ott, P, "Viscous and inviscid linear/nonlinear calculations versus quasi three-dimensional experimental cascade data for a new aeroelastic turbine standard configuration," *Journal of Turbomachinery*, Vol. 121, No. 4, October 1999, pp. 717–725.

[43] Elliott, J. and Peraire, J., "Constrained multipoint shape optimization for complex 3D configurations," *Aeronautical Journal* , Vol. 100, No. 1017, 1998, pp. 365-376.

[44] Gill, P.E., Murray, W. and Wright, M.H., "Nonlinear constraints," *Practical optimization*, 10th edition, Academic Press, San Diego, 1993, pp. 205-260.

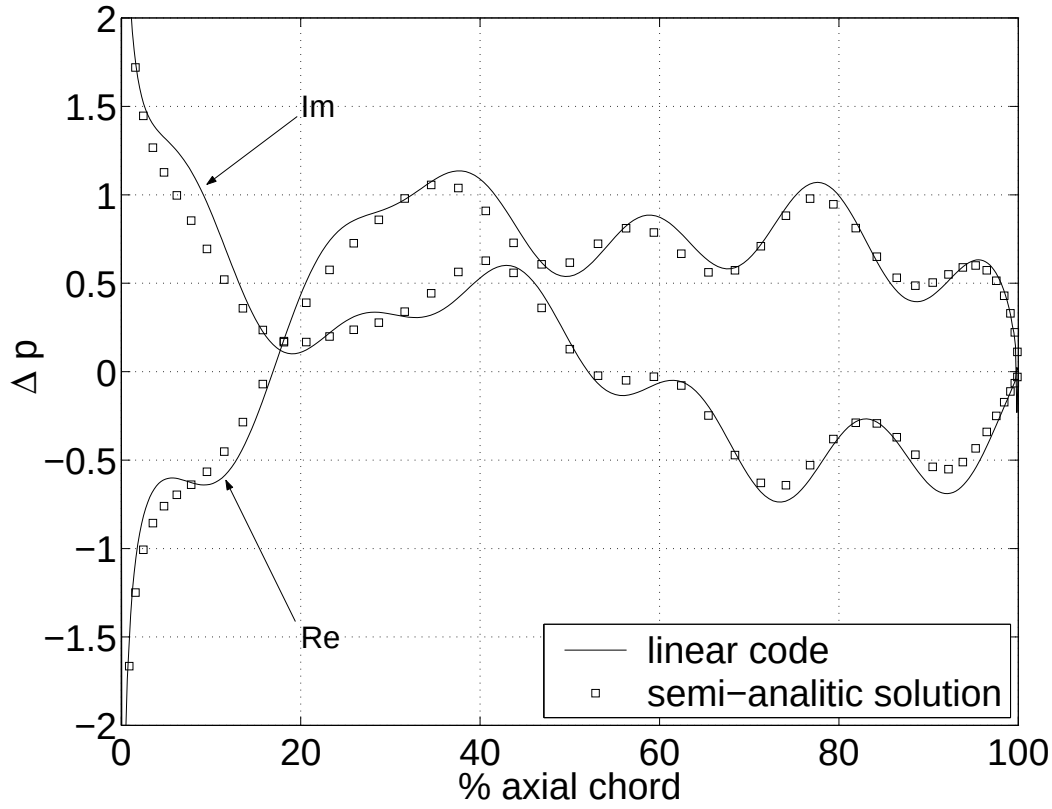

Figure 1: Real and imaginary part of the pressure difference across the unstaggered flat plates of a linear cascade due to incoming wakes with $IBPA = -400^0$.

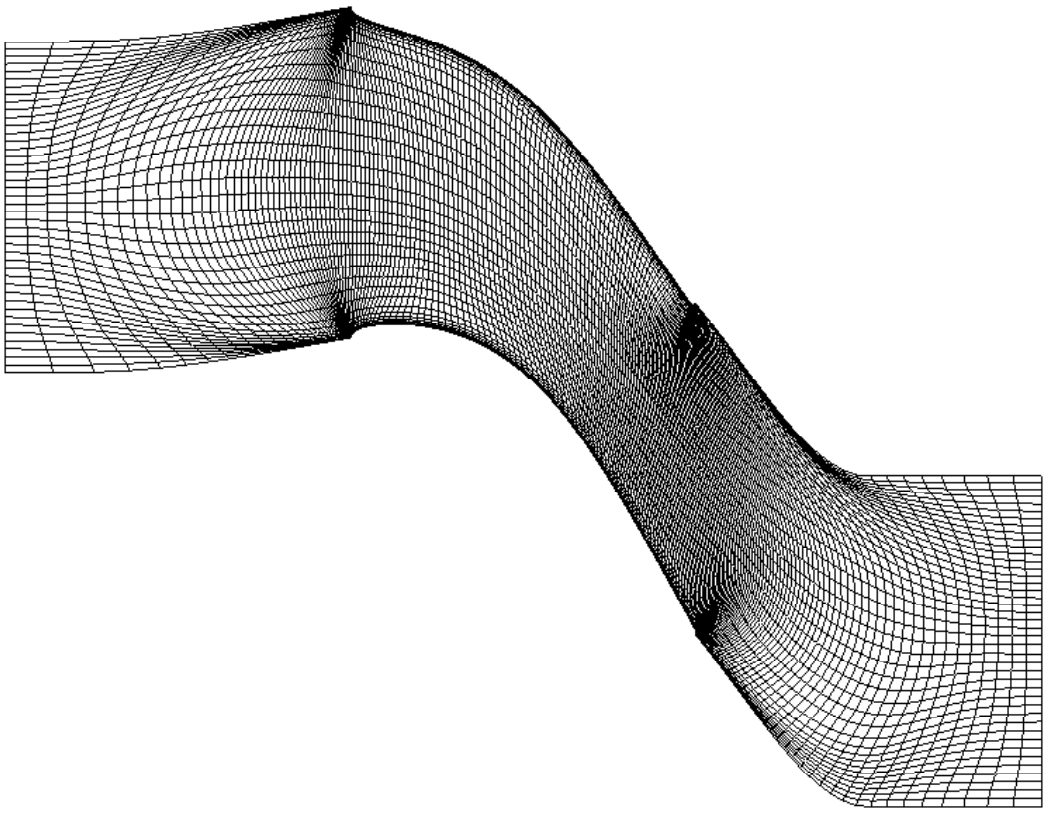

Figure 2: Coarse mesh for the 2D turbine of the 11th standard configuration.

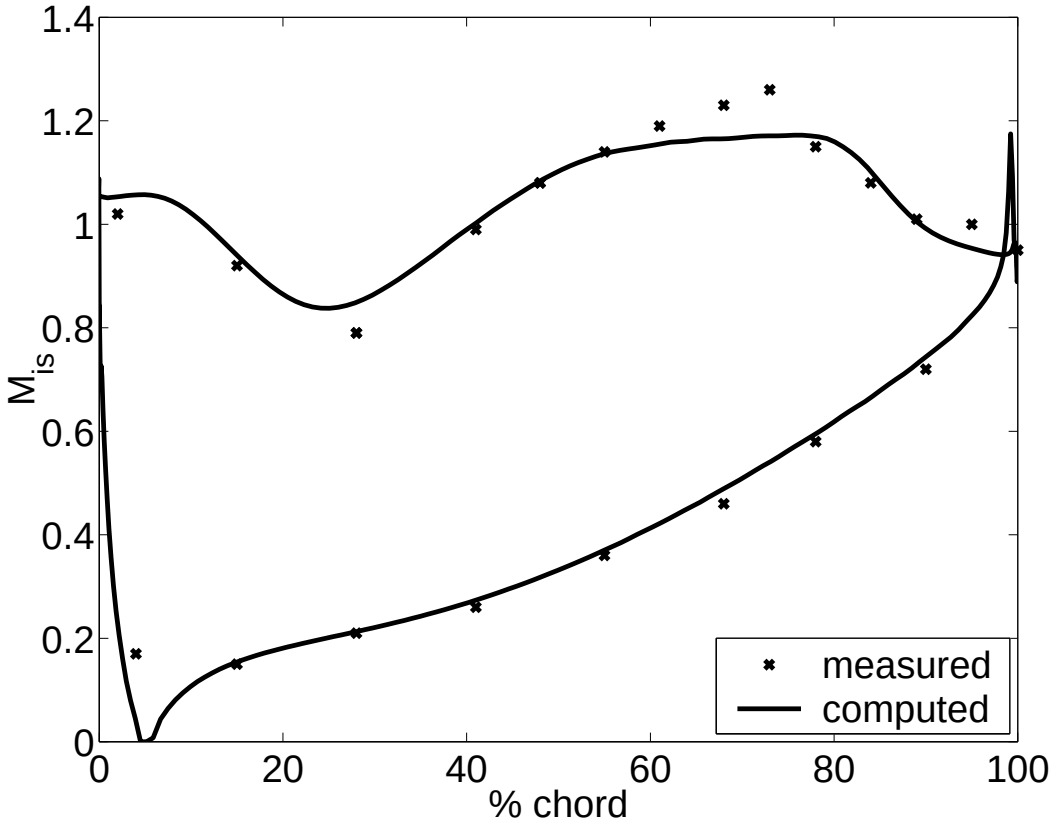

Figure 3: Isentropic Mach number on the blade surface of the 2D turbine for transonic working conditions.

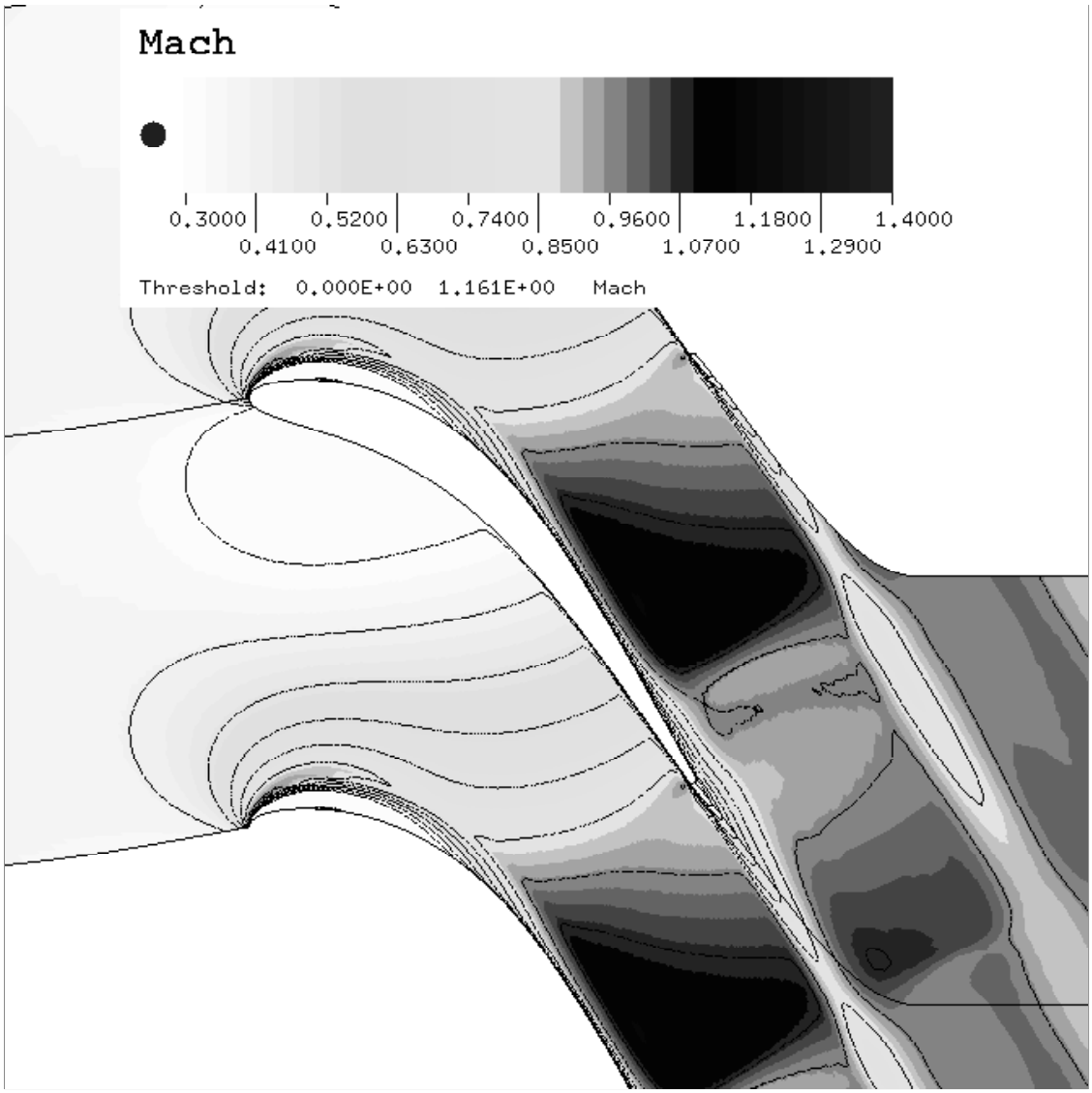

Figure 4: Mach contours for transonic conditions of the 2D turbine.

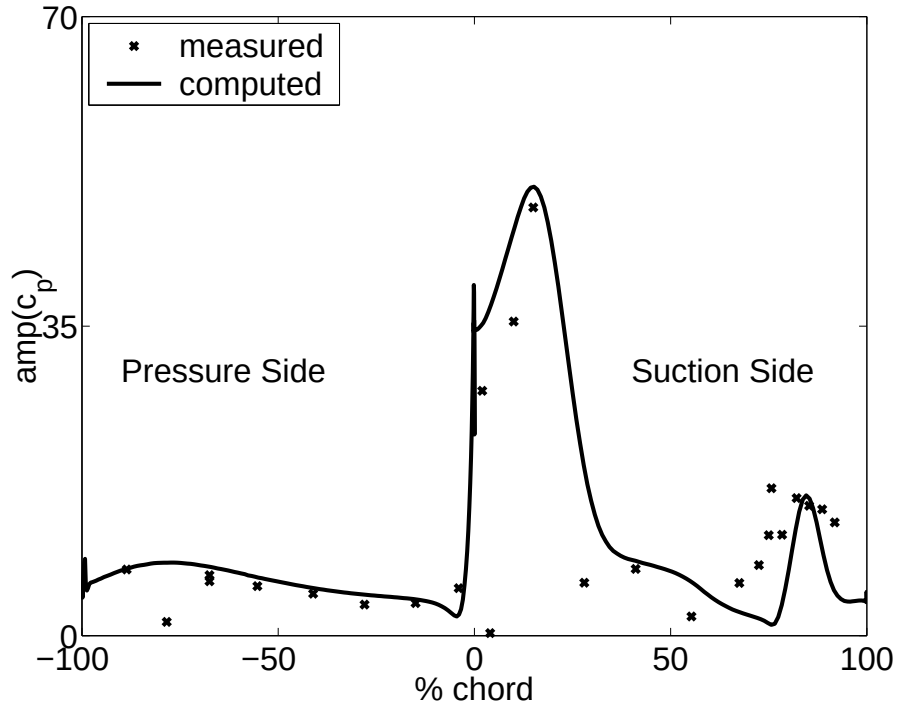

a)

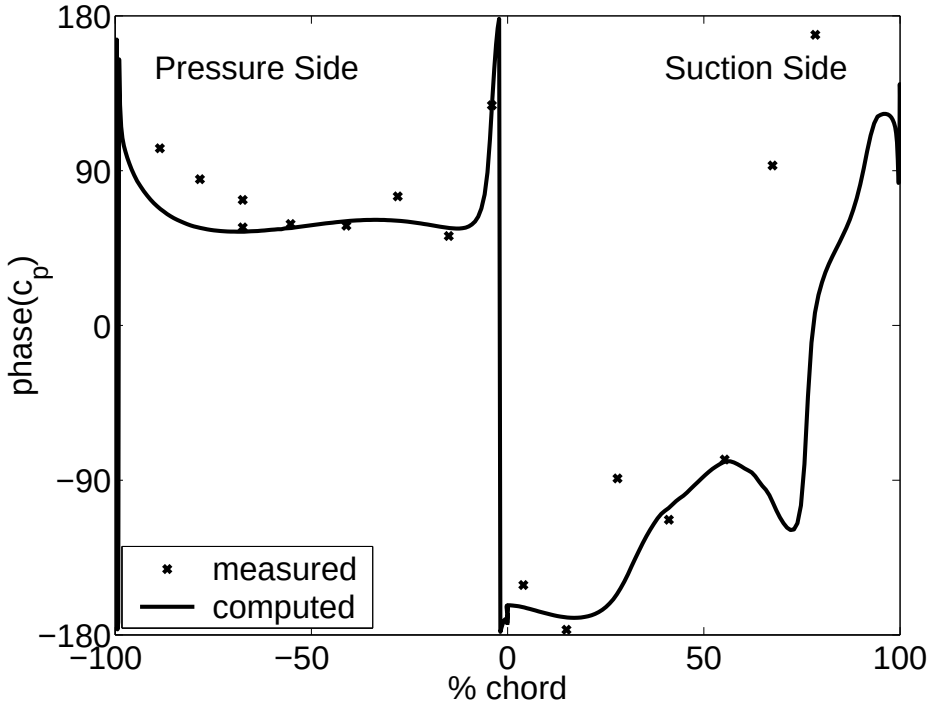

b)

Figure 5: *a*) Amplitude and *b*) phase of unsteady pressure coefficient c_p on the blade surface of the 2D turbine for transonic conditions and $IBPA = 180^o$.

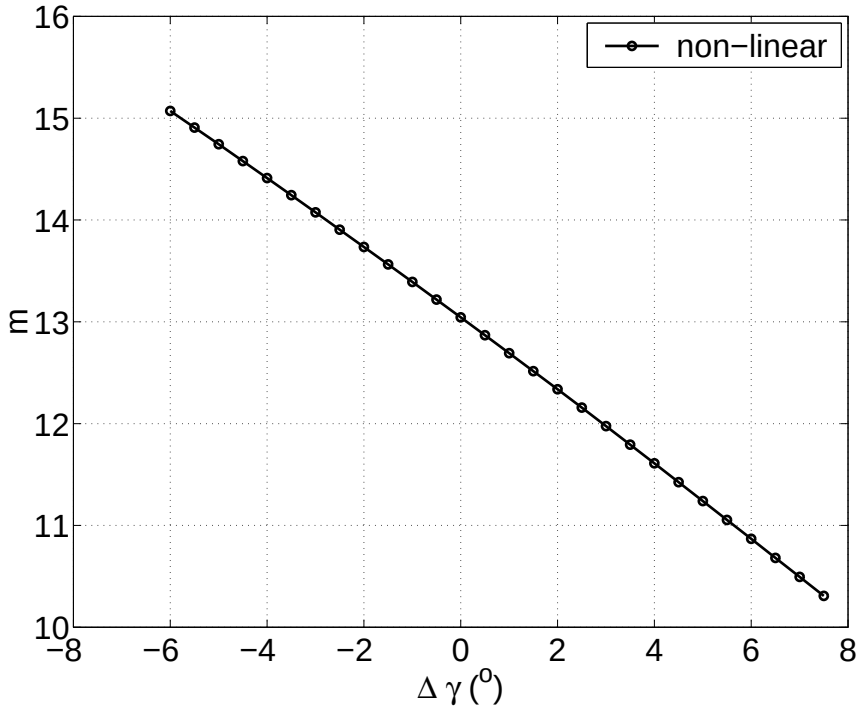

a)

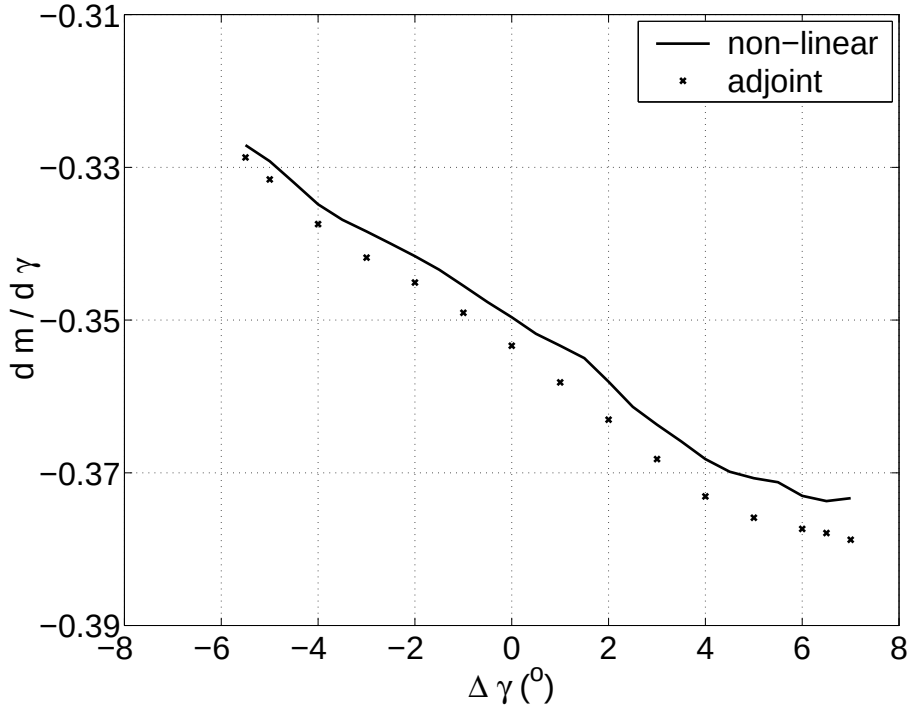

b)

Figure 6: *a*) Computed mass flow of 2D turbine versus variations of the stagger angle $\Delta\gamma$ and *b*) nonlinear versus adjoint mass flow sensitivity.

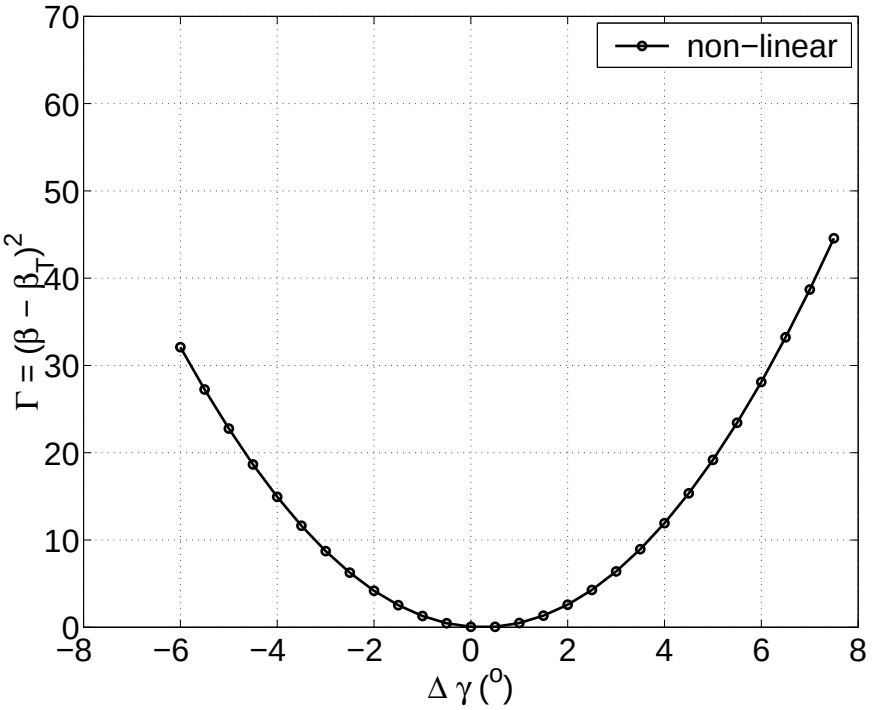

a)

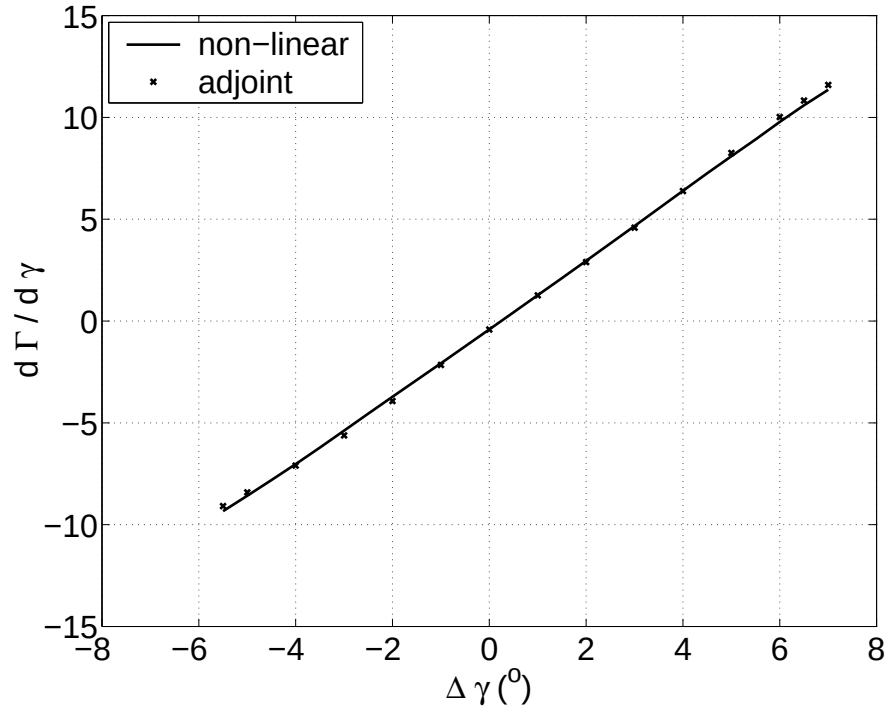

b)

Figure 7: *a*) Computed quadratic deviation $\Gamma = (\beta - \beta_T)^2$ of 2D turbine versus variations of the stagger angle $\Delta\gamma$ ($\beta_T = 58.6^o$) and *b*) nonlinear versus adjoint Γ sensitivity.

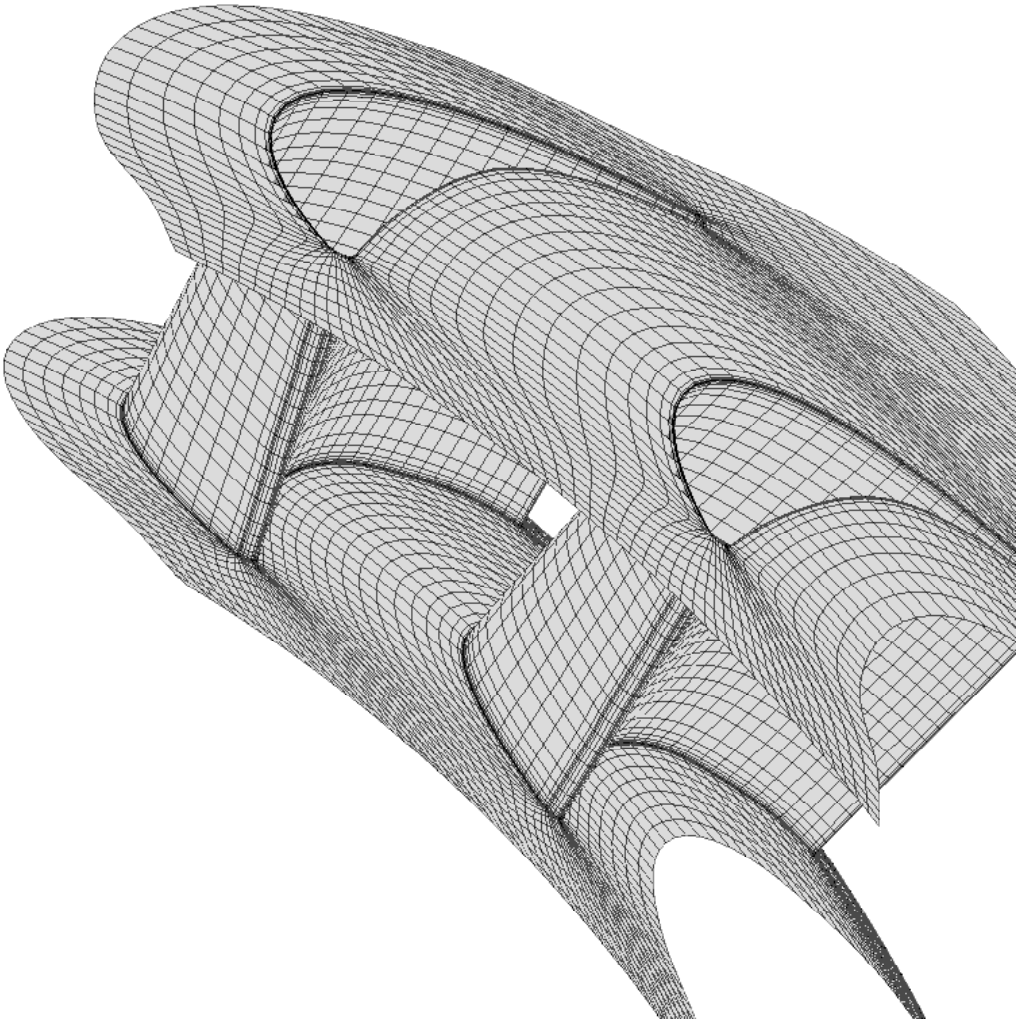

Figure 8: Unperturbed IGV geometry

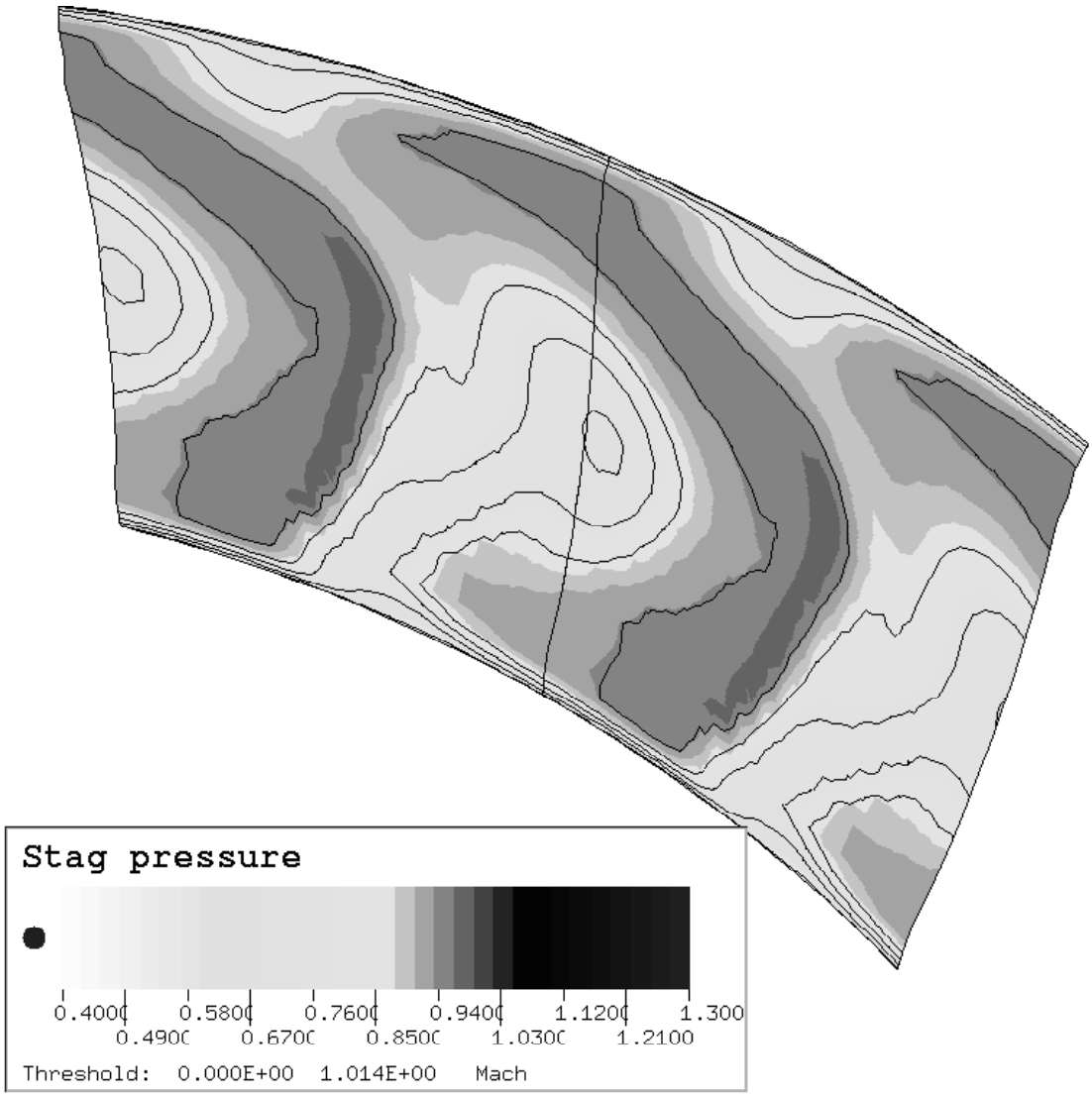

Figure 9: Contours of non-dimensionalized total pressure at turbine IGV outlet.

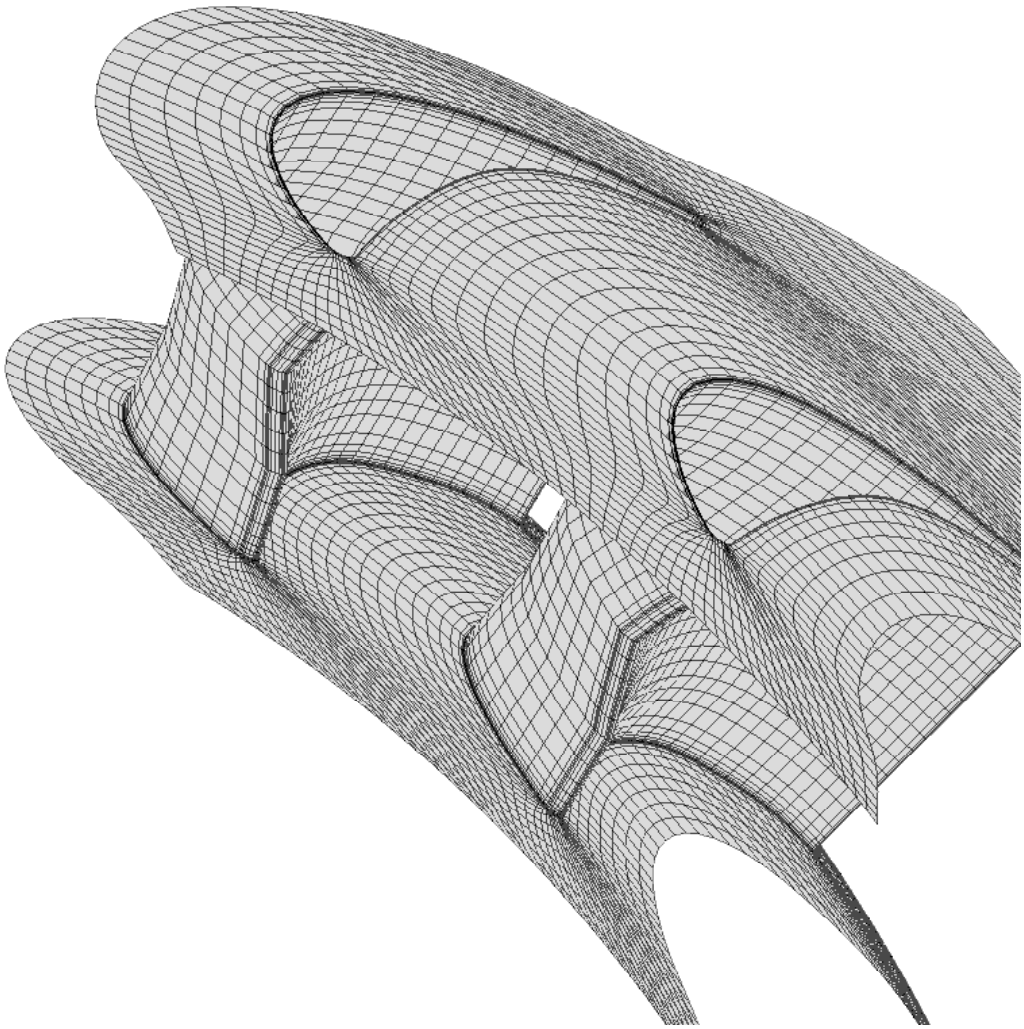

Figure 10: Perturbed IGV geometry

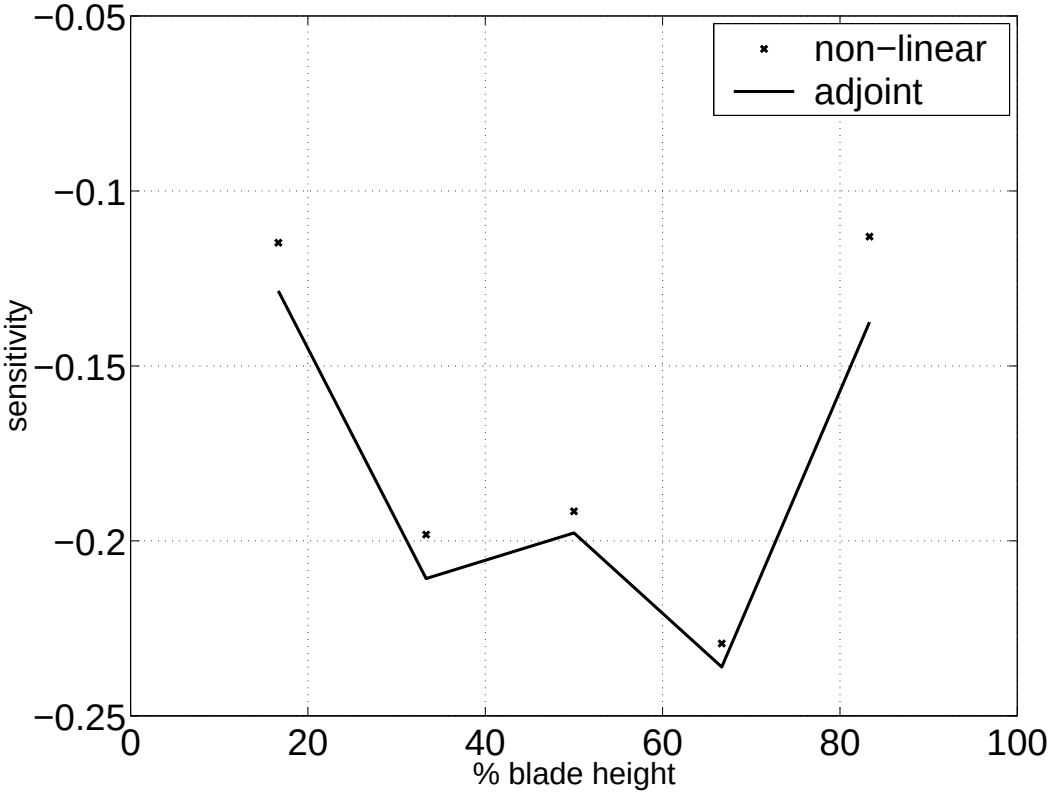

Figure 11: Mass flow sensitivity.

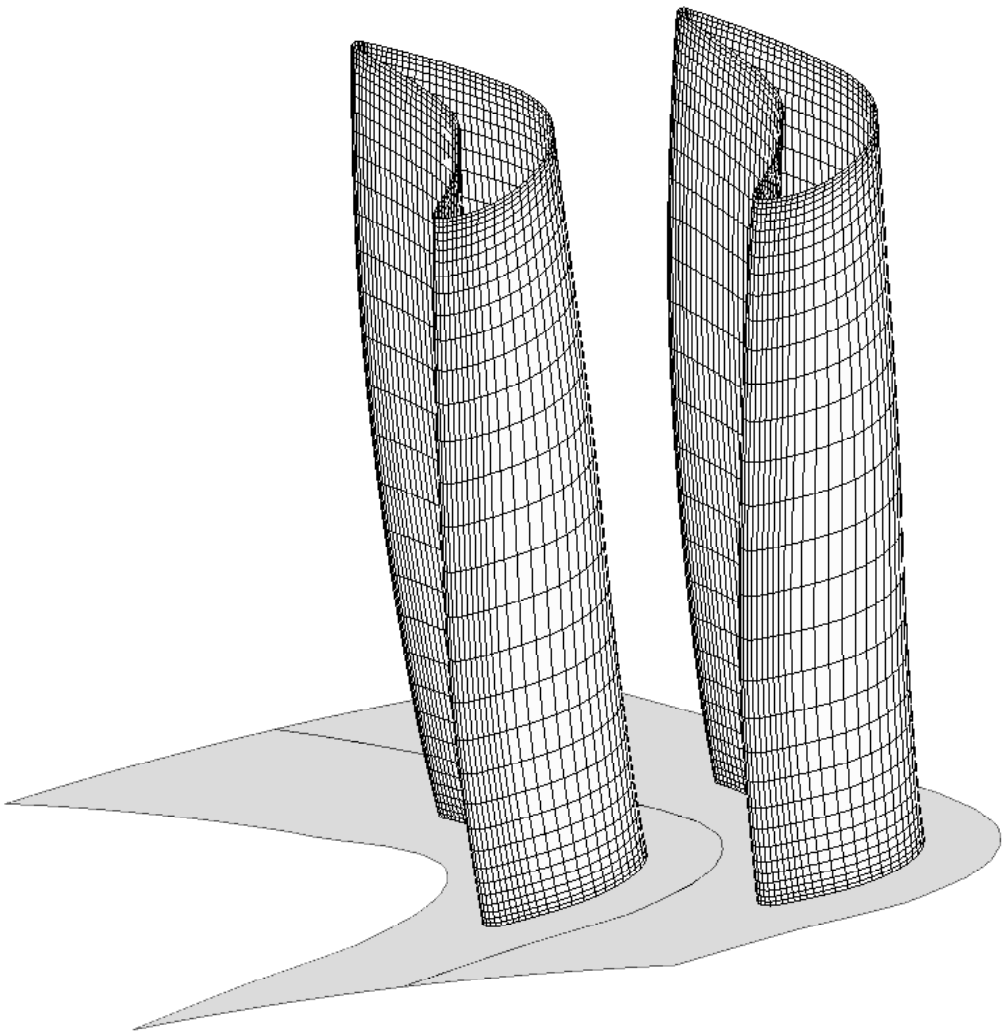

Figure 12: Geometry and grid surface of the turbine rotor.

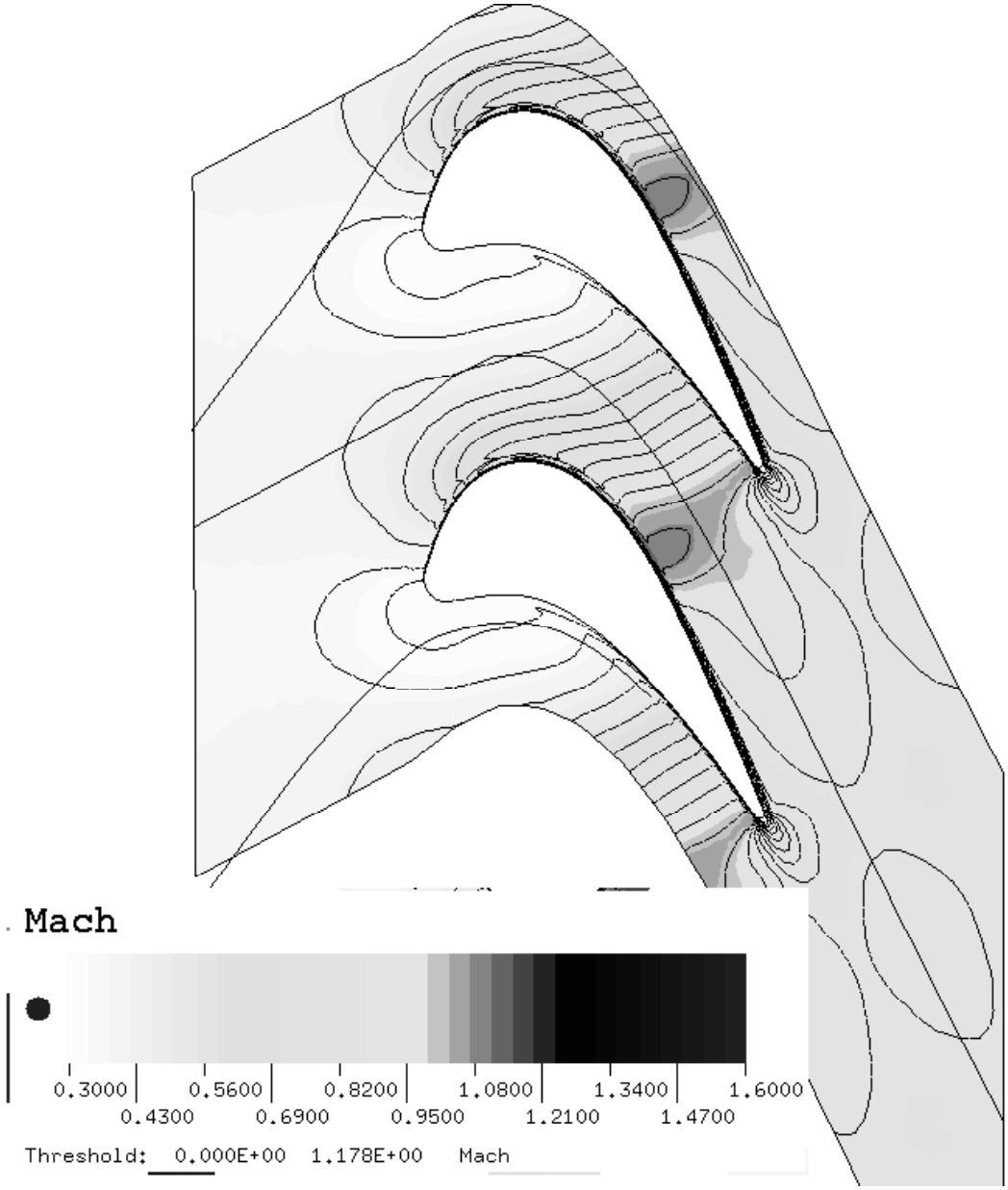

Figure 13: Mach contours in the mid-height blade-to-blade section of the turbine rotor.

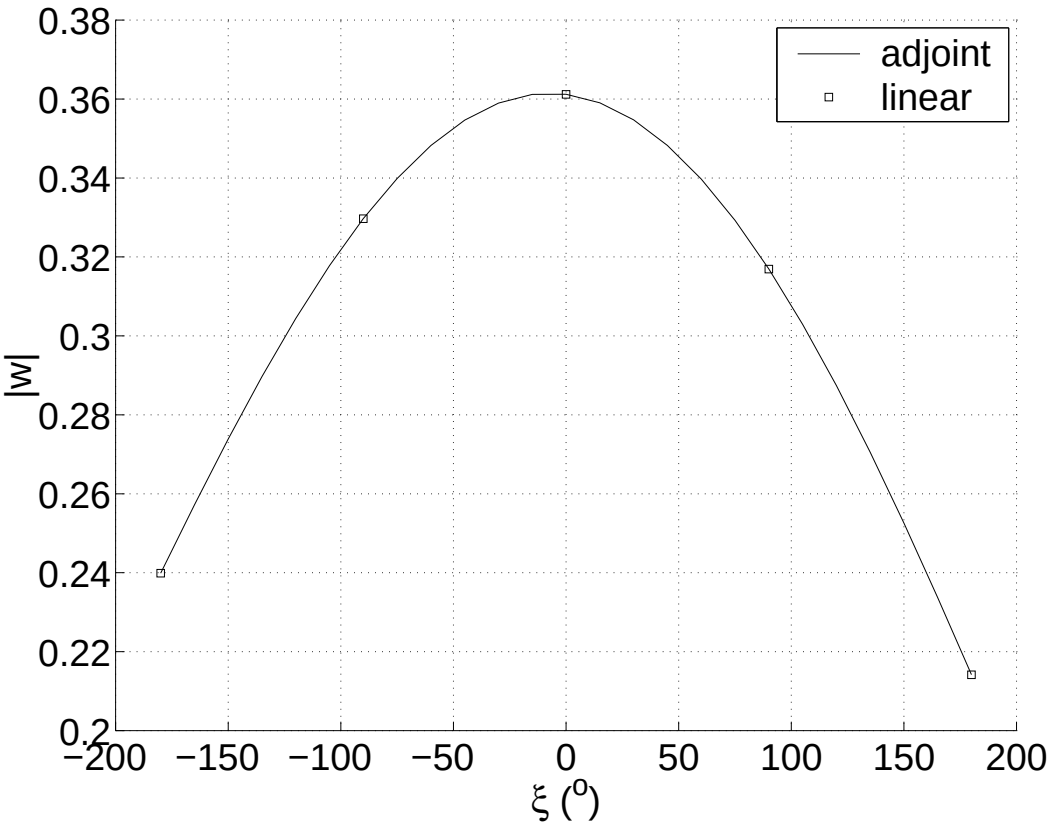

Figure 14: Forced response magnitude versus maximum re-stacking phase shift.